



Optimization of the CAMEA Triple Axis Spectrometer based on MC-simulations

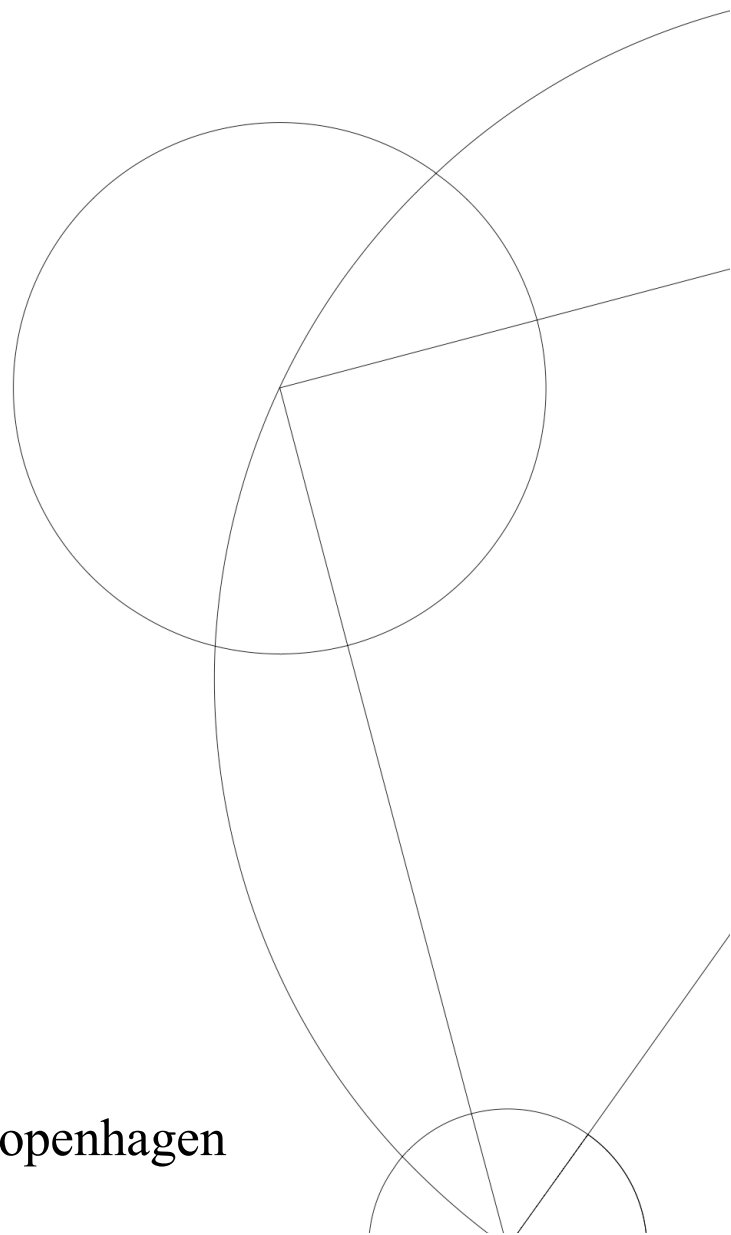
Bachelor project

Written by *Simon Kjær*

June 14, 2024

Supervised by Prof. Kim Lefmann
Co-supervised by Kristine M. L. Krighaar

University of Copenhagen





UNIVERSITY OF
COPENHAGEN

NAME OF INSTITUTE: Niels Bohr Institute - University of Copenhagen

NAME OF DEPARTMENT: Condensed Matter Physics

AUTHOR(S): Simon Kjær

EMAIL: qxg787@alumni.ku.dk

TITLE AND SUBTITLE: Optimization of the CAMEA Triple Axis Spectrometer
based on MC-simulations

-

SUPERVISOR(S): Kim Lefmann Co-supervisor: Kristine M. L. Krighaar

HANDED IN: 14.06.2024

DEFENDED: 27.06.2024

NAME _____

SIGNATURE _____

DATE _____

Acknowledgements

I would like to thank my supervisor Kim Lefmann for sharing his invaluable intuition for Neutron instrumentation, finding meaning and reason behind datasets I would never have discovered on my own. His immediate understanding made for a very productive workflow. I would also like to thank Kristine Krighaar for showing me the ropes of MCStas and sharing her tips and tricks to get the most out of my simulations. I cannot understate the importance of working in a group that is willing to help each other out. The sharing of knowledge between people in the Neutron group has been a huge help, on the numerous occasions when I got stuck. Last but not least I would like to thank my fellow students Lau Kartholm and Sebastian Bramman for providing fun breaks and useful discussions.

Abstract

This project utilizes the ray-tracing program McStas to rediscover and quantify an error on the Continuous Angle Multiple Energy Analysis (CAMEA) spectrometer. The current setup uses a slit 8 cm from the end of the guide as a virtual source for Rowland geometry, however, previous tests show that the beam naturally focuses at 47 cm from the end of the guide. An analysis of the beam profile shows that moving the slit to the focus point allows for a 22% increase in neutron flux. In the process of finding the full effect of this error, the simulations fail to establish consistency. The inconsistency is then by diagnostic simulations traced back to a fault in the Rowland Geometry of the MCStas component `Monochromator_curved`. The instruction manual does not match the calculations in the source code. A way to get optimal focusing from the component is to use the Rowland radii as input parameters `Rv` and `Rh` rather than the Radius of Curvature that the manual suggests. Because of the time spent finding the error, this project does not yet offer a full solution to the initial error.

Contents

1	Introduction	1
2	Theory	2
2.1	Theory of Neutron Scattering	2
2.1.1	Neutron as waves	2
2.2	Statistical	3
2.2.1	Inelastic scattering	5
2.3	Crystal Diffraction	6
2.4	Triple-Axis-Spectrometer	6
2.5	Rowland Geometry	7
3	Methods	8
3.1	McStas	8
3.1.1	McStas Calculations	8
3.2	CAMEA-Setup	9
4	MC Simulations of CAMEA-Setups	10
4.1	Analyzing the Beam Profile	10
4.1.1	partial-discussion	11
4.2	Scan of Slit-opening	12
4.2.1	Partial discussion	12
4.3	Scan of Monochromator Curvature	13
4.3.1	partial discussion	13
4.4	2-D Scan of Placement and Opening of Slit	14
4.4.1	partial discussion	15
5	Discussion	16
6	Conclusions	18
6.0.1	Future Work	18
	References	19

1. Introduction

One of the finest skills of the physical sciences is the ability to reliably build knowledge upon foundations laid by others. This requires extreme dedication to transparency and recreatability but creates an environment where the collective knowledge is ever-growing.

Continuing in the spirit of collaboration, this project starts where another ended. In a project from November, Kristine Krighaar found a concerning flaw in the setup of the CAMEA neutron spectrometer. A flaw that most certainly can be mitigated, and thus increase the efficiency of the neutron scattering instrument. [1]

In recent years the technique of neutron scattering has gained a lot of popularity in engineering, and biology on top of its usual followers from crystallography[2]. It has thus become increasingly important to create effective neutron experiments.

The Continuous Angle Multiple Energy Analysis (CAMEA) spectrometer is one of such facilities and is located at the Paul Scherrer Institute in Switzerland. CAMEA is groundbreaking in the sense that it combines a lot of new technologies such as the prismatic analyzer concept, multiplexing, and the double-focusing monochromator. This allows it to collect wider ranges of data at a fraction of the time. This instrument has tremendous potential and has yet to be fully optimized.

This project seeks to quantify the error found in [1] and the potential winnings of its solutions, by experimenting on a virtual copy of the CAMEA spectrometer. The ultimate goal is to provide enough knowledge on the error to decide if and how to modify the real instrument.

”If I have seen further than others, it is by standing upon the shoulders of giants.”

Isaac Newton, 1675

2. Theory

2.1 Theory of Neutron Scattering

The neutron is an electrically neutral particle with mass $m_n = 1.6749 \times 10^{-27}$ kg. Neutrons do not exist naturally in free form as they will decay into a proton, electron, and electron anti-neutrino with a decay time $\tau_n > 14$ min, and since a standard scattering experiment takes less than a second, the lifetime is not something that will be further considered.

Neutrons interact with nuclei through the strong nuclear force and the electromagnetic force. The electromagnetic interaction is because of neutrons' magnetic moment. These interactions have a very small radius and make neutrons ideal for probing the bulk of crystals or very light atoms like hydrogen.

Neutrons are subatomic particles and therefore abide by the rules of Quantum mechanics. This puts the uncertainty principle into consideration

$$\Delta x \Delta p \geq \frac{\hbar}{2} \quad (2.1)$$

A quick calculation reveals that this is not going to be an issue at all. The neutrons move on the order of 10^3 m/s, they weigh on the order of 10^{-27} kg and the interactions happen on the order of millimeters (10^{-3} m). Revealing $10^{-27} \geq 10^{-34}$ kg m^2/s , we pass by order of millions of \hbar . This puts us in the semi-classical regime meaning that we can think of the neutron as classic particles, but quantum mechanics dictate the intricacies of the interactions.

2.1.1 Neutron as waves

An incoming neutron is generally described by complex plane-wave[3]

$$\psi_i(\mathbf{r}) = \frac{1}{\sqrt{Y}} e^{i\mathbf{k}_i \cdot \mathbf{r}} \quad (2.2)$$

Here Y is a normalization constant, it is here to be consistent with general QM results, but will eventually cancel out. \mathbf{k} is the wavevector which points in the direction of velocity. More specifically \mathbf{k} is represented with the following relations.

$$k = \frac{2\pi}{\lambda} = \frac{m_n v}{\hbar} \quad (2.3)$$

In the case of such a neutron wave hitting a single atom you get a spherical diffraction

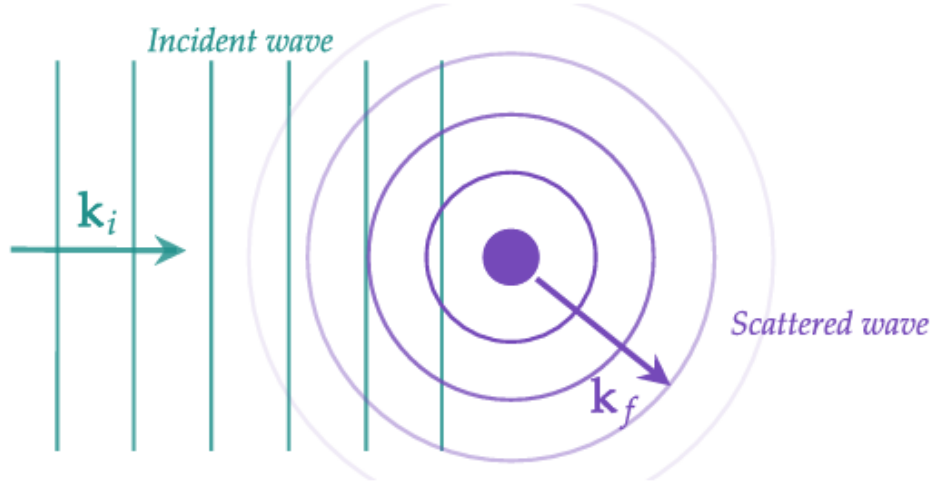


Figure 2.1 Neutron scattering of a single nuclei. The plane wave of the initial neutron (green) with wave number k_i scatters of the nuclei (purple), creating a spherical scatted wave with wave number k_f [4]

as shown in fig. 2.1. Such a scattered wave would relate to the incoming wave by eq.28

$$\psi_f = \psi_i \frac{-b_j}{|\mathbf{r} - \mathbf{r}_j|} e^{ik_f|\mathbf{r} - \mathbf{r}_j|} \quad (2.4)$$

2.2 Statistical

This section closely follows derivations from Chapter 2 in [3]. In the case of neutron beams, we want to examine how eq. 2.4 translates into multiple neutrons. We replace a single neutron with a neutron flux, which we define as

$$\Phi = \frac{\# \text{ neutrons per second}}{\text{surface area perpendicular to beam}} \left[\frac{n}{m^2} \right] \quad (2.5)$$

From this, we get the scattering cross-section naturally as

$$\sigma = \frac{\# \text{ of neutrons scattered}}{\Phi} [m^2] \quad (2.6)$$

This quantity is central to neutron scattering because it describes the probability of an incoming neutron scattering off a sample. It does this with a unit of area, which for a single atom will roughly equal the cross-section of the nucleus. It is often useful to compare the cross-section with experiments, but since we rarely see detectors completely surrounding the

sample, it is effective to use the differential scattering equation.

$$\frac{d\sigma}{d\Omega} = \frac{1}{\Phi} \frac{\# \text{Number of neutrons scattering into } d\Omega}{d\Omega} \quad (2.7)$$

$d\Omega$ is a section of the sphere surrounding the sample such that if we were to integrate over 4π it would completely enclose the sample as illustrated in fig. 2.2. This means that the differential cross-section and scattering cross-section is related (rather trivially) by.

$$\sigma = \int_{4\pi} \frac{d\sigma}{d\Omega} d\Omega \quad (2.8)$$

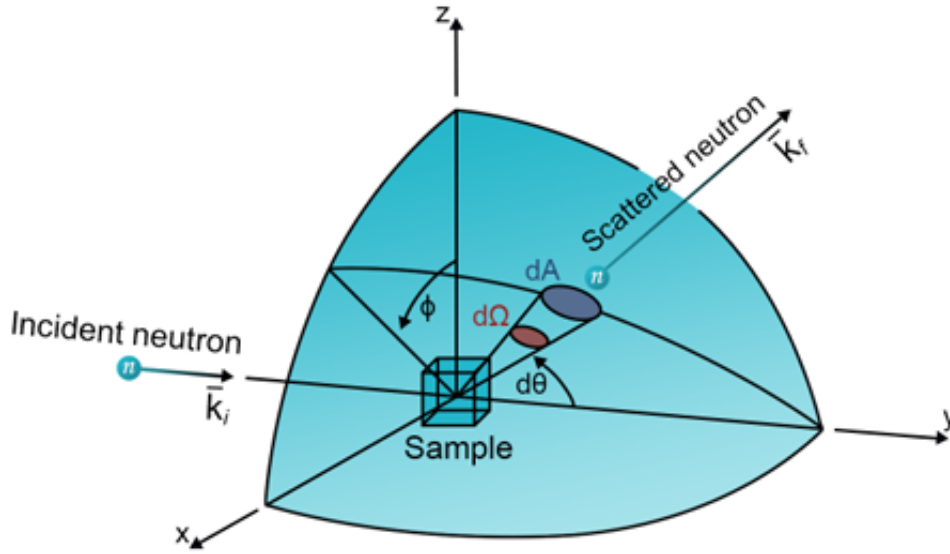


Figure 2.2 An illustration of incoming neutron, labeled k_i , scattering off a sample in the center and leaves as outgoing neutron k_f . It scatters with the scattering angle 2θ ($d\theta$ shows the plane in which it is measured) and azimuthal angle ϕ . dA represents a detector and $d\Omega$ is the associated solid-angle. [3]

we have now established two fundamental concepts in neutron scattering; the scattered neutron spherical wave and the differential scattering equation, and it is time to unite the two. In Quantum Mechanics the density of a neutron wave is $|\psi|^2$, which means that the flux is $|\psi|^2 v dA$. Seeking to fuse with eq. 2.7 we use the defining expression for the solid angle $d\Omega = \frac{dA}{r^2}$ and the expression of flux through an area $v |\psi|^2 dA$, combining these we get $\# \text{neutrons into } d\Omega \text{ pr. sec} = v |\psi|^2 r^2 d\Omega$. Recalling the wavefunction from 2.4 we get

$$\# \text{neutrons into } d\Omega \text{ pr. sec} = v |\psi_i(\mathbf{r}) \frac{-b_j}{|\mathbf{r} - \mathbf{r}_j|} e^{ik_f |\mathbf{r} - \mathbf{r}_j|} |^2 r^2 d\Omega \quad (2.9)$$

Putting the origin of coordinates inside the sample typically gives $r_j \simeq 1 \mu m$ and $r \simeq 1 \text{ m}$, making it reasonable to remove r_j from the equation. Taking the absolute value of complex exponentials returns 1, which leaves us with only b_j^2 , v , and the normalization

constant from ψ_i .

$$\#neutrons \text{ into } d\Omega \text{ pr. sec} = v \frac{b_j^2}{Y} d\Omega \quad (2.10)$$

isolating v in eq. 2.3 gives $v = \frac{k\hbar}{m_n}$

$$\#neutrons \text{ into } d\Omega \text{ pr. sec} = \frac{k_f \hbar}{m_n} \frac{b_j^2}{Y} d\Omega \quad (2.11)$$

In this example, we assume a fixed target and thus $k_i = k_f$, which we can utilize to substitute in an expression of total flux $\Phi = v_i |\psi_i|^2 = \frac{k_i \hbar}{m_n} \frac{b_j^2}{Y}$

$$\#neutrons \text{ into } d\Omega \text{ pr. sec} = \Phi b_j^2 d\Omega \quad (2.12)$$

$$\frac{\#neutrons \text{ into } d\Omega \text{ pr. sec}}{\Phi d\Omega} = b_j^2 \quad (2.13)$$

lastly, we substitute in eq. 2.7 to get a the beautifully simple expression:

$$\frac{d\sigma}{d\Omega} = b_j^2 \quad (2.14)$$

2.2.1 Inelastic scattering

In some scattering processes the neutron delivers or absorbs energy, these are often the most interesting when probing a sample. If we differentiate our measurements based on energy, meaning we only count neutrons with a certain energy, our theory needs to account for that as well. We denote energy transfer as

$$\Delta E = E_{initial} - E_{final} = \hbar \omega \quad (2.15)$$

When a detector measures a neutron with a given energy, what it actually measures is the amount of neutrons passing through the detectors solid angle, called **Partial differential cross section**.

$$\frac{d\sigma^2}{d\Omega dE_f} = \frac{1}{\Phi} \frac{\#flux \text{ trough } d\Omega \text{ with energies } \in [E_f; E_f + dE_f]}{d\Omega} \quad (2.16)$$

We get the regular differential cross section by integrating over all energies

$$\frac{d\sigma}{d\Omega} = \int_0^\infty \frac{d\sigma^2}{d\Omega dE_f} dE_f \quad (2.17)$$

2.3 Crystal Diffraction

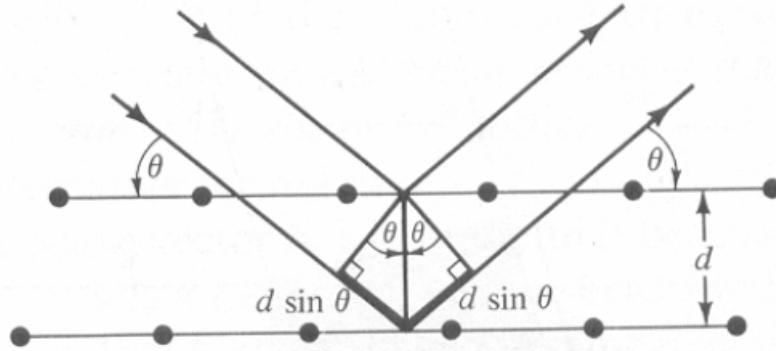


Figure 2.3 Incoming neutron wave hits lattice planes and reflects. d denotes the distance between lattice planes, and θ is the scattering angle.

In our experiments, we usually interact with crystal lattices. Imagine a crystal lattice as shown in fig. 2.3 an incoming plane wave hits the first layer and is partly reflected, other parts of the wave penetrate the first layer, but are reflected at the next lattice plane. The deepest wave will now have traversed a longer distance equal to $2d \sin \theta$. This gives rise to interference, which will be constructive if the extra distance equals an integer of the wavelength. **Bragg's law.**

$$n \lambda = 2d \sin \theta \quad (2.18)$$

This will prove to be incredibly useful when picking out and narrowing down the energy resolution of neutron waves.

2.4 Triple-Axis-Spectrometer

Recalling from the inelastic scattering that we are often interested in the energy deposited in the sample. To measure this we need to know as precise as possible both the initial energy and the final energy. Triple-axis-Spectrometers (TAS) can offer this from a continuous beam of Neutrons, contrary to other experiments which requires a 'chopper' to block off 95% of the beam to choose energy based on Time of Flight measurements.

TAS chooses energies by utilizing Bragg's law since different energy neutrons have different scattering angles (see eq. 2.18). This reflective apparatus is (very fittingly) called a monochromator. Moving on the neutron hits and scatters of the sample with a scattering angle depend on the q -vector (read more in [3]). The Neutrons now hit an analyzer, similar to the monochromator the neutrons scatter at different angles according to their energy. This allows us to measure multiple final energies and still differentiate between them. The three axes are capable of, first singling out initial energy, secondly rotating the sample, and lastly rotating analyzers to measure multiple final energies and thus also deposited energies.

2.5 Rowland Geometry

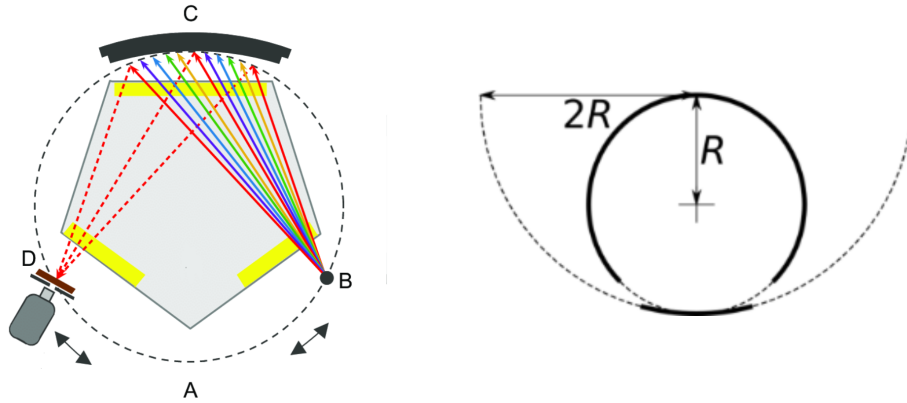


Figure 2.4 (left) [5] A) the dotted line shows the Rowland circle on which a focus point in (D) will mimic the focusing of a source or slit (B), C) is Spherical Bent Analyzer or Monochromator. (Right) Shows the relation between the Rowland circle (solid) and the Radius of Curvature of the diffraction grating (dotted).

Rowland geometry is crucial in optimizing intensity and energy resolution for neutron scattering. A study from 2012 found increases up to 43% increase in intensity and energy resolution, and a general increase for all cases (the study varied the asymmetry of distance from source to monochromator and monochromator to sample)[6]. Rowland geometry dictates geometrically, that a source with distance R to a monochromator will focus a distance R after reflecting if the monochromator is spherically bent to a curvature of 2R as illustrated in fig. 2.4

Often we won't have direct knowledge of the radius of the Rowland circle, but by geometry we can deduce the radius R of the circle that contains the source, monochromator and target in its peripheral. [5]

$$R = \frac{L}{\sin\theta} \quad (2.19)$$

where L is the distance from the source to the monochromator. Since the scattering angle is determined by bragg-scattering it depends on the wavelength which is proportional to the energy of the neutrons. We can then determine the radius of the Rowland circle by.

$$R = L \sin(\theta) \quad , \quad \theta = \arcsin \frac{1}{0.1106\sqrt{E_i} 2d} \quad (2.20)$$

Where E_i is the energy of incoming neutrons, and d is the distance between lattice planes. 0.1106 is a conversion factor from inverse wavelengths in \AA^{-1} to squareroot of energy in $\text{meV}^{\frac{1}{2}}$. [3] Remember now that the radius, R, above is the Rowland circle, and the optimal radius of curvature for focusing is 2R. [3]

3. Methods

This project is a series of analyses determining the effects of changes on a virtual copy of the CAMEA instrument. Some are motivated by theories regarding optimizing energy resolution, and other simulations are for diagnostic purposes following unexpected results. The analyses are Monte-Carlo Simulations in the Ray-tracing program McStas.

3.1 McStas

MCStas is a program, that does Monte-Carlo simulations of neutrons as ray tracings. It runs as a C-code program but is fully accessible through a Graphical User Interface (GUI). MCStas is perfect for this project because it combines the practical reality of an experimental setup, with the intricacies of microscopic adjustments. Through the GUI you can build a virtual neutron scattering setup by placing components by their coordinates in a virtual landscape. The GUI contains a large menu of components I.E: Sources, Samples, Guides, Monochromators, and PSD (positional sensitive detectors). Each of these components is equipped with extensive customizability.

3.1.1 McStas Calculations

A standard neutron facility can emit up to 10^{15} neutrons per second. Which is much more than any standard computer can simulate in a year[7]. For this reason, it is advantageous to simulate a single ray containing multiple neutrons. We denote this as p_i describing the amount of neutrons in the i 'th ray. Imagine now this ray interacting with a component, j , and some neutrons may be lost, we assign a weight multiplier, ω_j to the interaction that changes p_i .

$$p_{i,j} = \omega_j p_{i,j-1} \quad , \quad \omega_j f_{mc,b} = P_B \quad (3.1)$$

Here the equation to the right expresses the correlation between ω , the probability of event B, P_B , and the sampling probability $f_{mc,b}$

We can now define the intensity at a certain point as the sum of p-values for all the rays at this point in the experiment [7]

$$I_j = \sum_{i=1}^N p_{i,j-1} \quad (3.2)$$

We can determine the uncertainty on the Intensity by the following derivation. Imagine M rays each with probability P_d of reaching the intensity detector. The number of rays will be normally distributed with mean value $\bar{N} = MP_d$ and variance $\sigma^2(N) = M P_d(1 - P_d)$,

in our experiments we can always expect $p_{dij} \ll 1$ and $M \gg 1$. This leads us to an expression for std. [8]

$$\sigma(N) = \sqrt{M P_d} \simeq \sqrt{N} \quad (3.3)$$

Where N is the best observed measurement for a mean. Now if all p -values are equal, meaning the path to the detector is distinct, eq. 3.2 transforms to the following with the corresponding variance

$$I = Np \quad , \quad \sigma^2(I) = Np^2 \quad (3.4)$$

Which generalizes to

$$I = \sum_{i=1}^N p_i \quad , \quad \sigma^2(I) = \sum_{i=1}^N p_i^2 \quad (3.5)$$

Which is easier for the program to store, by summing the p_i and p_i^2 while running.

3.2 CAMEA-Setup

The CAMEA instrument is a cutting-edge neutron spectrometer and is very technical in every aspect, but to keep relevance I will only go into explicit detail with the monochromator.

Neutrons are released from accelerated protons colliding with lead. A surrounding layer of deuterium slows the neutron down to manageable energy levels [3,14]meV. A monolith is then used to single out neutrons with the desired energy and let them enter the guide. The guide utilizes double elliptical geometry to increase the critical reflection angle and maximize neutron flux. [9] [10]. The elliptical shape of the guide gives rise to a virtual source, a point of focus, between the end of the guide and the monochromator. [10]

8 cm from the end of the guide is a slit that serves to block out pollution from higher-order scattering. It is adjustable in its opening [3]

160 cm from the end of the guide is a monochromator, specifically a large double-focusing monochromator. It is made up of $15 \times 15 \times 2 \text{ mm}^3$ Highly ordered Pyrolytic Graphite (HOPG) single crystals with a d-spacing of 3.355 \AA . The crystals are arranged with a mosaicity of $0.6^\circ - 0.8^\circ$, arranged in 11 rows and 17 columns, spanning a total area of $173 \times 262 \text{ mm}^2$. The monochromator is flat but can approximate the Rowland focusing by tilting each plate accordingly. [10]

160 cm downstream from the monochromator is the sample, from where the neutron are scattered onto analyzers. The CAMEA-spectrometer is fairly unique in the sense that multiple analyzers are spread out like a fan and layered to probe a larger range of Q-values or Energies depending on the experiment.

The detectors themselves are helium tubes using Time of Flight to determine energy levels. [10]

4. MC Simulations of CAMEA-Setups

The motivation for this project is based on earlier findings from Kristine Krighaar, where an analysis by Positional Sensitive Detector (PSD) showed that the placement of the slit does not align with the focus of the beam, which could be a cause for concern. We start the optimization process by rediscovering the misalignment.

4.1 Analyzing the Beam Profile

To visualize the beam and possibly discover a misalignment of components, I want to get a visualization of the beam. I place a PSD, which can be thought of as a non-interacting chessboard perpendicular to the beam that measures intensity in each square. The PSD is $20 \times 20 \text{ cm}^2$ and 100×100 pixels. Then all real-world obstructions are removed and 100 of these PSD are placed between the end of the guide and the monochromator (1.6m downstream). To visualize the data in a readable manner, I sum the intensity on all y-columns and plot it as a color plot as a function of the x-axis and the distance from the guide-end. This will visualize as the beam intensity seen from above as shown in fig. 4.1

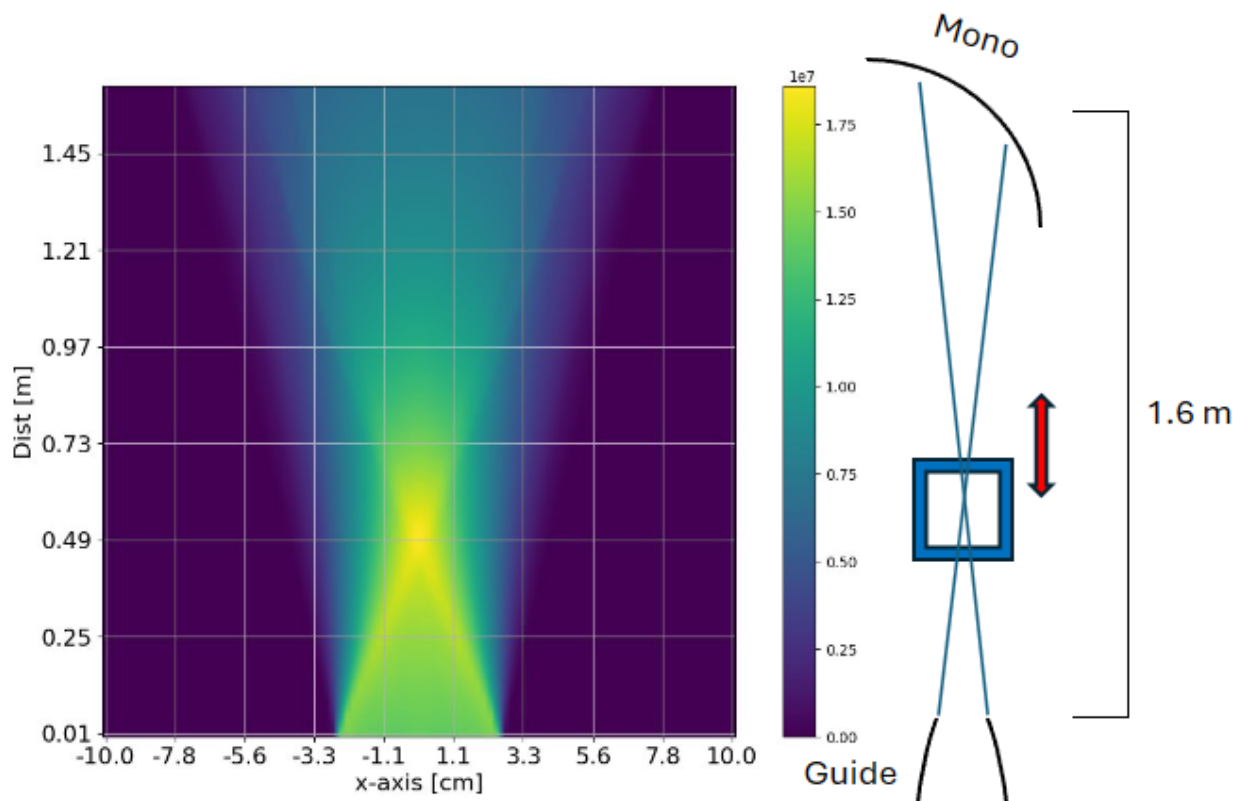


Figure 4.1 (left) This figure shows the intensity of the beam between guide-end and monochromator as seen from above. The intensity shown is the sum of the intensity in the vertical columns gained from a Positional Sensitive Detector. (Right) Shows an illustration of how the data was gained, the blue square illustrates a PSD.

From fig. 4.1 it looks as if a 1 cm opening at an 8 cm distance will block a substantial amount of neutron flux, which will amount to less experimental data and be sub-optimal. To get quantification on the matter we make two slices through fig. 4.1 as close to 8 cm (7.4) as possible and another slice where the peak in center intensity is the highest (47.4 cm). We then plot it intensity as the y-axis and the x-axis as the spatial dimension. We then make binned integral, summing up the intensities between -0.5 cm and 0.5 cm, to find the intensity passing through a 1cm slit. The ratio between these intensities is the percentage increase we expect to gain if the slit is placed 40 cm further downstream. This is illustrated in fig. 4.2.

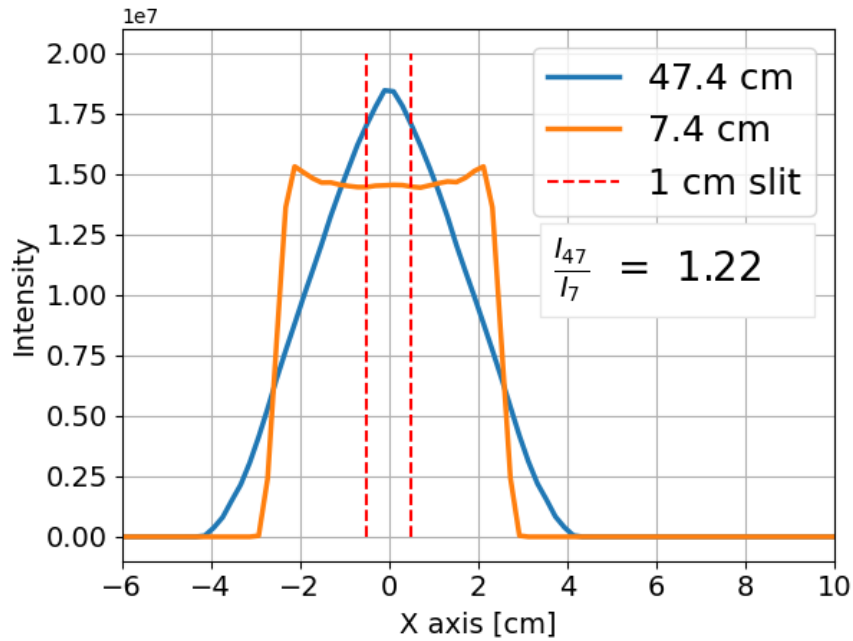


Figure 4.2 This figure shows intensity profiles of a $E_i = 5$ meV neutron beam at 47.4 cm (blue) and 7.4 cm (orange) downstream from the guide-end. The intensity is the sum of all the vertical intensity for each pixel along the x-axis. The dotted red line illustrates the part of the profile that would pass through a 1 cm slit. The ratio calculated is the summed intensity inside the dotted line with 7.4 cm as the denominator.

4.1.1 partial-discussion

We have now shown that moving the slit 40 cm downstream can increase the intensity of the flux by 22% on the first part of the neutron beam. This does not necessarily increase the flux on the sample by this amount. We have yet to determine how this affects and plays together with the rest of the setup.

4.2 Scan of Slit-opening

In an attempt to gain knowledge on how a moved slit will affect the sample position, we put an energy monitor on the sample position that measures intensity and energy resolution. I will then create a setup with only a slit and a monochromator, and let the slit gradually open. I will do this experiment for both the 8 cm and 46 cm distances respectively. In both cases, there will be 1.6 m between the slit and monochromator as well as monochromator to sample to make a symmetric Rowland geometry.

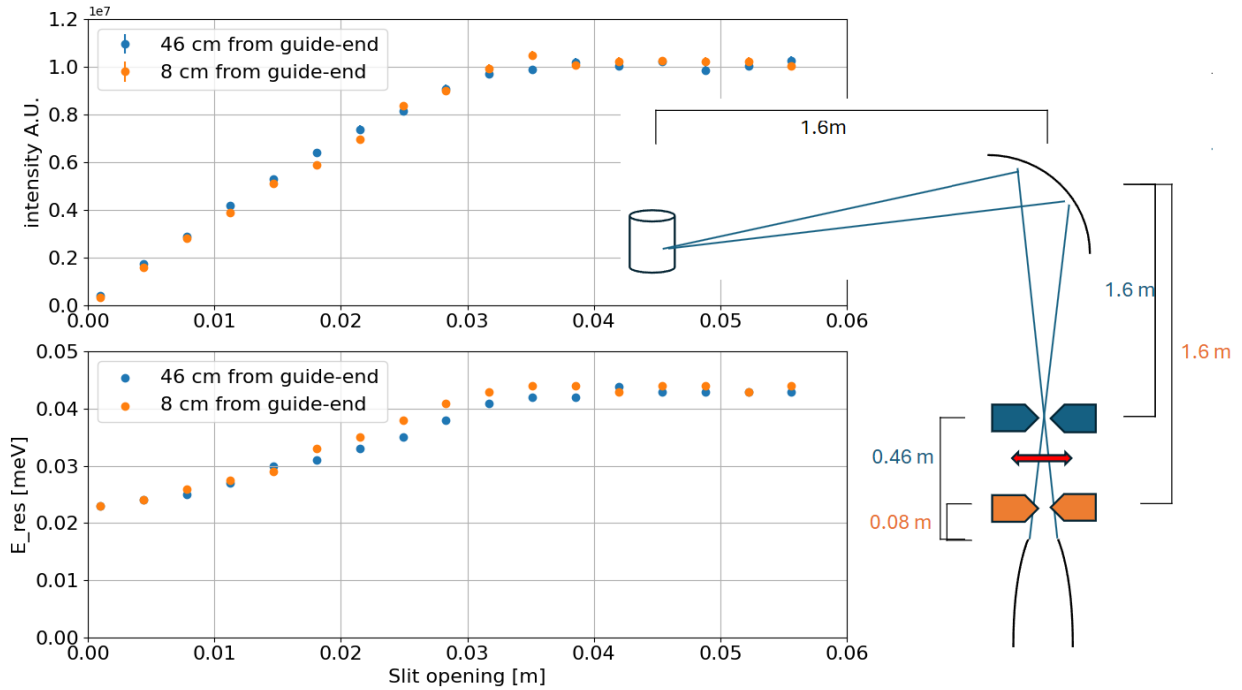


Figure 4.3 This figure shows Intensity (top) and energy resolution (bottom) as a function of gradually opening a slit at respectively 8 cm (blue) and 46 cm (orange) downstream from guide-end. simulation is done at $E_i = 5$ meV The right side is an illustration of the simulation.

4.2.1 Partial discussion

From this simulation we only see very little difference between placing the slit at 46 cm compared to the current 8 cm. Between a 1cm opening and 2.5 cm opening the slit furthest downstream gives rise to a small increase in intensity, nowhere near the 22%. Between 1.9 cm and 3.5 cm opening, the resolution is better for the 46 cm slit. This effect is expected since we know that a larger flux passes through, though we would expect this effect to diminish before reaching a 3cm opening. The fact that the 22% does not translate to the sample suggests two things. First whatever causes this, affects the experiment with the slit at 46 cm more than it affects the experiment with the slit at 8cm, since it skews the ratio

between these two. Secondly, the monochromator, and propagation length are the only things introduced, so likely one of them plays a role in this effect.

4.3 Scan of Monochromator Curvature

The monochromator was the only thing added when the difference in slit placement no longer made a significant impact. Because of this, we examine the Rowland geometry more closely. The Rowland geometry hinges on the radius of curvature being right and is normally calculated by eq. 2.17, in this simulation we bypass the calculation and use 21 given values for the radius of curvature. For each one, we measure the intensity on the sample position. We then see if the best radius of curvature matches what is normally calculated. We measure intensity with an e-monitor $2 \times 2 \text{ cm}^2$ at the sample position.

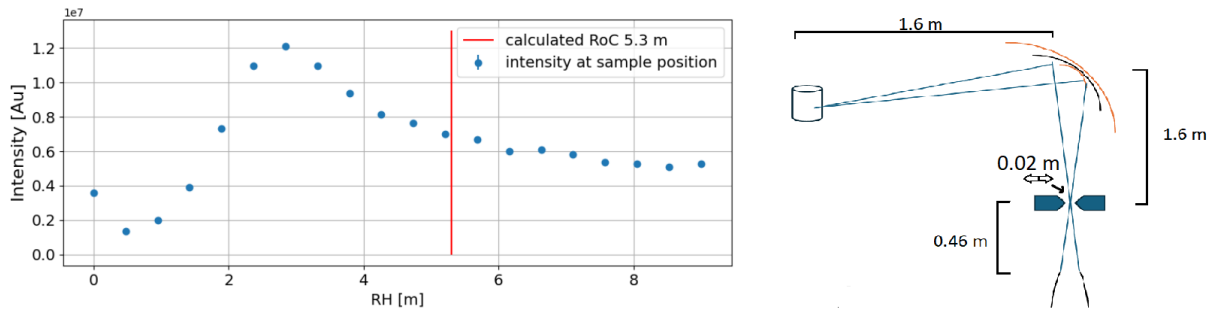


Figure 4.4 This figure shows intensity at a sample position when varying the radius of curvature on the monochromator, a red line indicates the calculated curvature that would lead to best focusing. To the right is a sketch of the setup with measurements.

The radius of curvature that yields the highest intensity does not match our calculations. We simulate a symmetric Rowland setup and with $E_i = 5 \text{ meV}$, where the distance from a virtual source to monochromator and monochromator to sample both are 1.6 m. The datapoint with the highest intensity has a radius of curvature (RoC) of 2.8 while calculations by eq. 2.17 (using 3.355 \AA as d-spacing and 5 meV as energy) yields 5.3 m as RoC.

4.3.1 partial discussion

From the eq. 2.17 there are only two things I decide when simulating; the incoming energy and the distance to the monochromator. When reading out the data, during this simulation, the incoming energy was set to 5 meV all the time. Which leads us to believe that something is wrong with the geometry of the setup. Calculating backwards with 2.8 m as RoC gives 0.85 m as the symmetric distance to the monochromator. For good measure, I will share the calculations here:

$$\theta = \arcsin \frac{1}{0.11056 \sqrt{5} \times 2 \times 3.355} = 0.647 \text{rad} \quad (4.1)$$

$$RoC = \frac{2 \times 1.6}{\sin \theta} = 5.3 \text{m} \quad (4.2)$$

The backward calculation:

$$\frac{2.8}{2} \sin(\theta) = 0.85 \quad (4.3)$$

Now I can't find any physical reason for these divided results, but I will speculate. The 2.8 max isn't very accurate since the gap between data points is almost 0.5 m, if we imagine the actual maximum is at $RoC = 2.65$ m we are exactly a factor 2 from the calculations, likewise, it would change the backward calculation to 0.8 m a factor 2 off from the actual distance. We know from Chapter 2.5 that there is a factor 2 between Rowland Radius and Radius of Curvature, which could've easily been mixed up.

After thoroughly combing through the McStas code, I can say with confidence that the virtual monochromator is used as intended. This indicates that the component manual and the actual source code does not match. I speculate that when programming the RoC it got mixed up with the Rowland Radius.[11].

4.4 2-D Scan of Placement and Opening of Slit

Throughout the project, there has been a lot of scanning over parameters, thus far one at a time. In this last simulation, the aim is to do one simulation that reveals the best place and opening width of a slit. This requires scanning over two parameters simultaneously, which can be achieved with a shell script. This shell script is a piece of code that runs the McStas program back-to-back, this way the McStas only scans one parameter, but as soon as it is done it starts again but with another parameter slightly changed. We do distance from the guide-end 5 cm to 55cm with 5 cm steps For each distance, we scan from 0 to 5 cm slit opening For all parameter combination the intensity and resolution is measured at sample position by a 2 x 2 cm² E-monitor. This experiment keeps symmetric Rowland Geometry by always keeping 1.6 m between the slit and monochromator. The results are shown in fig. 4.5

The 3-d plot shows no distinct optimal point, but the 2-d plot shows slightly better results for the 45 cm. Especially around 2 cm opening where the 45 cm has both higher intensity and lower Energy resolution.

4.4 2-D Scan of Placement and Opening of Slit

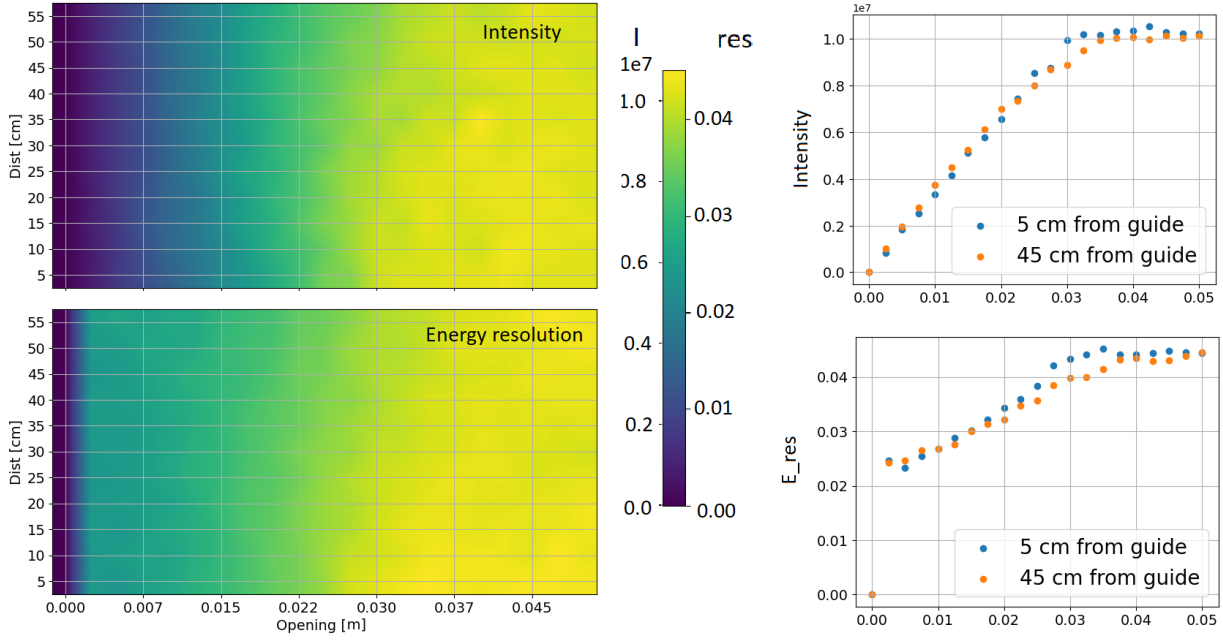


Figure 4.5 This figure shows intensity (top-left) and energy resolution (bottom-left) at the sample position measured with a 2×2 cm² E-monitor, it shows how these vary when a slit gradually opens at different distances from the guide-end. The Right side shows the same data, but as 2-d plot for 5 cm and 45 cm.

4.4.1 partial discussion

If moving the slit downstream would make an impact, we would see the color change being diagonal, which we do not. However, there is a small difference that can be seen on the 2-D plot albeit far from 22% but in line with the beam being more compressed at 45 cm than at 5 cm. It would seem that something happens at the monochromator which doesn't equally affect a simulation with a slit 5cm from the guide-end and a simulation 45 cm from the guide-end, since we see a reduction in the percentage diff in intensity. A quick speculation could be that moving the monochromator further downstream would allow the beam to spread more which might have a negative effect on the focusing. If this is the case then we would see the effect for all slit-opening sizes, but the data seem to converge on the right side of the plots in fig. 4.5, which debunks the theory.

5. Discussion

Having done multiple simulations it is now time to look at what they collectively point at. At first, we saw that moving a 1cm open slit from 8 cm to 47.4 cm downstream of the guide will increase the neutron flux by 22%. This effect almost completely disappeared when we introduced the monochromator, leading us to believe something was wrong. By simulating a large range of Radius of Curvature and matching them with what we normally would use by calculating, we find a clear misalignment of a factor 2.

When we use $L = 1.6$ m we get $\text{RoC} = 5.3$, the simulations show optimal $\text{RoC} = 2.8$ corresponding to $L=0.85$. Already here I speculated that the instructions and calculations on the component manual were wrong because of the almost perfect factor 2 difference.

From fig. 4.3 and fig. 4.5 we no longer see a 22% increase in flux. This indicates that the error affects the 45cm harder than the 5 cm. Which fits the RoC theory very well. Recalling from fig. 4.1 that the beam naturally focuses around 47 cm, we can imagine that introducing a slit upstream of this focus doesn't remove the focal point, what does change is the actual distance from the focus to the monochromator. The setup is such that the distance from slit to monochromator is 1.6 m which makes the distance from focus to monochromator 1.19 m for a 5 cm slit ($1.6\text{m} + 0.05\text{m} - 0.46\text{m} = 1.19$) which puts us closer to the optimal L value of 0.85. This theory is illustrated in fig. 5.1

We must consider that the second argument fig. 5.1 now deals with asymmetric Rowland geometry. In (Skoulatos, 2012) they simulate asymmetric Rowland and use $R = \frac{L_1+L_2}{2\sin\theta}$ [6]. Which in this case yields a RoC of 4.6 m instead of 3.9 m. Which fits very well. This theory seems to offer an explanation across multiple simulations, which makes it convincing

Reading out the nearest data point from fig. 5.1 gives $\text{RoC} = 5.3 \Rightarrow I = 0.69\text{e}7$, and $\text{RoC} = 4.6 \Rightarrow I = 7.8\text{e}7$. This would result in an equalizing effect of $\frac{6.9}{7.8}$ Which means that instead of seeing 22% increase, we should see $1.22 \times \frac{6.9}{7.8} = 1.079$. A 7.9% increase in intensity by moving the slit downstream, if the program is off by a factor of 2. Looking at fig. 4.3 and taking the ratio between the data points with a 1.1 cm opening we get $\frac{4.19\text{e}6}{3.90\text{e}6} = 1.074$. This shows that the theory establishes coherence between the simulations. Which then reinforces the idea that the methods used are correct beside the faulty calculations.

The faulty Radius of Curvature and its relation to all of the simulations was first realized within the last 48 hours of the project, the time restriction on the project dictates that there is no time to redo the simulations. To correctly find and quantify the optimal setup for the frontend slit we should use the Rowland radius as the input parameters for the component

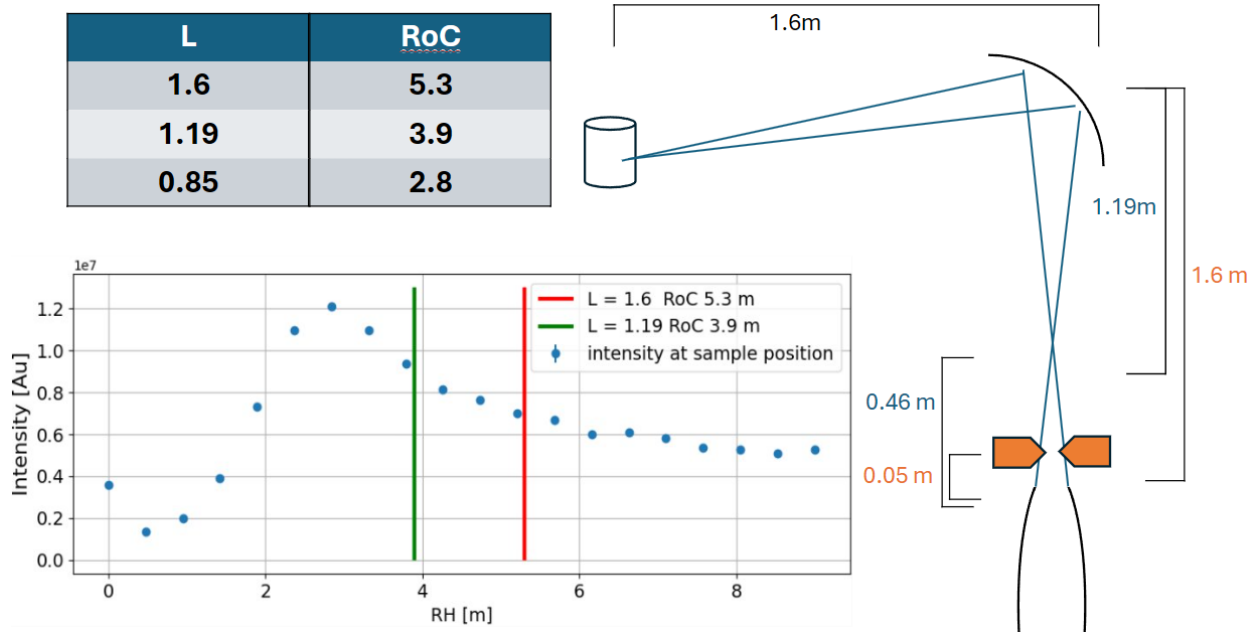


Figure 5.1 This figure illustrates a theory of how keeping the slit close to the guide-end causes better neutron flux because of faulty Rowland calculations. Upper left is a table showing the connection between distance from focus to monochromator (L) and Radius of Curvature (RoC) for 5meV and d-spacing = 3.355 Å. At the lower left is shown how intensity 1.6m downstream of the monochromator varies with RoC. The right side illustrates the setup with measurements.

monochromator_curved. Given as following

$$Rh = \frac{L}{\sin(\theta)} \quad Rv = L \times \sin(\theta) \quad (5.1)$$

Rh denotes the horizontal rowland radius, and Rv is the vertical rowland radius.

6. Conclusions

From analyzing the the beam profile between the guide-end and monochromator we find that the beam focuses around 47 cm downstream after the guide-end. If, instead of placing a slit at 8 cm like the current setup, the slit is moved to 47 cm, it would allow for a 22% increase in the Intensity of the neutron flux. Measuring the intensity at the sample position 1.6 m downstream of the monochromator does not seem to replicate the same result. This leads us to believe something is wrong with the virtual monochromator.

A further investigation unveils this fault to be a mismatch between the instruction manual and the source code of the component "monochromator_curved". More specifically the manual asks to use the Radius of Curvature as input parameters but calculates according to Rowland radius. The relation between these two is $RoC = 2 \times R_{rowland}$.

Because a slit can be thought of as a virtual source, we set up symmetric Rowland geometry by keeping an equal distance, equal to 1.6m, between slit and monochromator, and monochromator and sample. However because the beam naturally focuses at 46 cm downstream of the guide-end, a slit placed upstream of this point will have an actual shorter distance between the virtual source and monochromator, leading to a more accurate Rowland Geometry when using the faulty input parameters. As an example if a slit at 46 cm allows for an immediate 1.22 times more neutron flux than a slit at 5cm. The monochromator will focus better in the 5cm scenario and reduce this ratio to 1.068. This explains why measurements on the sample position failed to replicate the same increase in flux from moving the slit downstream.

To find the optimal placement of a slit between guide-end and monochromator, the input parameters Rv and Rh of component Monochromator_curved need to be the radius of the corresponding Rowland circle, not the Radius of Curvature.

$$Rh_{rowland} = \frac{L}{\sin\theta} \quad , \quad Rv_{rowland} = L \times \sin\theta \quad (6.1)$$

6.0.1 Future Work

First and foremost this fault in the component manual of MCStas will be reported to the MCStas team as a bug.

The future work on optimizing the CAMEA spectrometer, in regards to the slit position will be quantifying the potential gain in intensity and energy resolution on the sample position when moving the slit downstream and using correct Rowland geometry. Then in correspondence with the people at PSI figure out if and how this could be implemented.

References

- (1) Krighaar, K. M. L. the energy resolution function for the CAMEA neutron spectrometer, November 2023.
- (2) Lefmann, K. e. a. *Journal of Neutron Research*,97-111 **1 Jan. 2008**.
- (3) Lefmann, K., *Neutron Scattering Theory, Instrumentation, and Simulation Lecture notes*; (University of Copenhagen: Sept. 2023.)
- (4) Krighaar, K. ADigital Twin of the BIFROST Neutron Spectrometer at ESS, MA thesis, Niels Bohr Institute - University of Copenhagen, 3. may - 2024.
- (5) Mottram, L.; Cafferkey, S.; Mason, A.; Oulton, T.; Sun, S.-K.; Bailey, D.; Stennett, M.; Hyatt, N. *Journal of Geosciences* **2020**, *65*, 27–35.
- (6) Skoulatos, M.; Habicht, K.; Lieutenant, K. *Journal of Physics: Conference Series* **2012**, *340*, 012019.
- (7) Willendrup, P. K.; Lefmann, K. McStas (i): Introduction, use, and basic principles for ray-tracing simulations, 2020.
- (8) R.J., B., *Statistics: a guide to the Use of Statistical Methods in the Physical Sciences*; Wiley: 1989.
- (9) www.PSI.ch The SINQ facility , <https://www.psi.ch/en/bsq/sinq-facility>, 2017 , read 2024-6-10.
- (10) Lass, J. et al. *Review of Scientific Instruments* **2023**, *94*, 023302.
- (11) Emmanuel Farhi Kim Lefmann, P. L. *The Monochromator_curvedComponent*, <https://www.mcstas.org/download/components/3.4_current/optics/Monochromator_curved.html>; tech. rep.; ILL, Aug. 24th 2001.
- (12) Brangwynne, C. P.; Eckmann, C. R.; Courson, D. S.; Rybarska, A.; Hoege, C.; Gharakhani, J.; Jülicher, F.; Hyman, A. A. *Science* **2009**, *324*, PMID: 19460965, 1729–1732.